Synthesis and in-vitro antibacterial properties of the novel Ag wires reinforced carbon based composite coatings

Ji, Xiaochao; Dong, Yangchun; Li, Xiaoying; Yu, Helong; Ma, Tian; Zhang, Wei; Dong, Hanshan

DOI:
10.1016/j.apsusc.2020.146207

Document Version
Peer reviewed version

Citation for published version (Harvard):
Ji, X, Dong, Y, Li, X, Yu, H, Ma, T, Zhang, W & Dong, H 2020, 'Synthesis and in-vitro antibacterial properties of the novel Ag wires reinforced carbon based composite coatings', *Applied Surface Science*, vol. 517, 146207. https://doi.org/10.1016/j.apsusc.2020.146207

Journal Pre-proofs

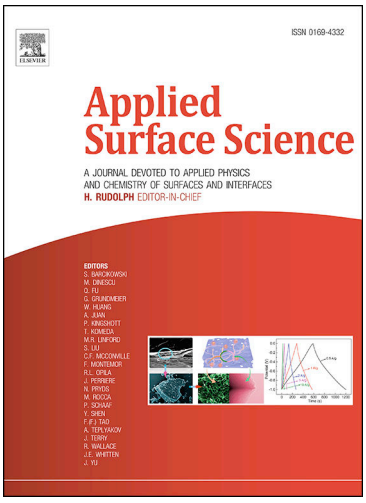

Full Length Article

Synthesis and in-vitro antibacterial properties of the novel Ag wires reinforced carbon based composite coatings

Xiaochao Ji, Yangchun Dong, Xiaoying Li, Helong Yu, Tian Ma, Wei Zhang, Hanshan Dong

PII: S0169-4332(20)30963-6
DOI: https://doi.org/10.1016/j.apsusc.2020.146207
Reference: APSUSC 146207

To appear in: *Applied Surface Science*

Received Date: 27 August 2019
Revised Date: 13 January 2020
Accepted Date: 24 March 2020

Please cite this article as: X. Ji, Y. Dong, X. Li, H. Yu, T. Ma, W. Zhang, H. Dong, Synthesis and in-vitro antibacterial properties of the novel Ag wires reinforced carbon based composite coatings, *Applied Surface Science* (2020), doi: https://doi.org/10.1016/j.apsusc.2020.146207

Synthesis and in-vitro antibacterial properties of the novel Ag wires reinforced carbon based composite coatings

Xiaochao Ji[a,b], Yangchun Dong[b*], Xiaoying Li[b], Helong Yu[c*], Tian Ma[a], Wei Zhang[d], Hanshan Dong[b]

[a]*Institute of Quartermaster Engineering & Technology, AMS, Beijing, 100010, China*
[b]*School of Metallurgy and Materials, The University of Birmingham, Birmingham B15 2TT, UK*
[c]*National Key Laboratory for Remanufacturing, AAAF, Beijing 100072, China*
[d]*Jingjinji Institute of Remanufacturing Industry & Technology, Hebei 062450, China*

Highlights:

- In-situ synthesis of the Ag wires through an AS plasma co-alloying process
- One-step approach to achieve the Ag wires reinforced composite coating
- Excellent antibacterial properties against *P. gingivalis* and *S. epidermidis* were achieved by the Ag wires reinforced composite coating.
- The vapor-solid growth mechanism is applied to explain the formation of the Ag wires.

Abstract: Novel Ag wires reinforced composite coating is developed using a novel active screen plasma co-alloying process in the plasma ambient of methane and hydrogen, and silver wires were *in-situ* formed through a sputtering process. Scanning electron microscopy and transmission electron microscopy were applied to investigate the microstructures of the Ag wires and the composite coatings. It revealed that the Ag wires were randomly embedded in the composite coating which were formed by aggregated nano-Ag, whilst the composite coating was formed with silver, stainless steel and carbon. X-ray diffraction and X-ray photoelectron spectroscopy (XPS) were utilised to characterise the phases and chemical states of the composite coatings, which verified the metallic form of Ag and non-chemical bond between deposited metals and carbon. A vapor-solid mechanism was applied to explain the growth of the Ag wires

during the duplex deposition. Excellent bactericidal effects of the composite coatings against both Gram-negative *P. gingivalis* and Gram-positive *S. epidermidis* bacteria were acquired through contacting with coated metallic samples.

Keywords: composite coating, silver wires, sputtering, active screen, plasma, antibacterial

1. Introduction

Novel composite coatings are attractive owing to their unique compositions and architectures. Various deposition techniques have been developed to deposit advanced composite coatings with specific properties that cannot be achieved by conventional single component coatings [1]. Studies and developments on architectures of novel composite coating have provided a theoretical basis to design composite coatings with extraordinary mechanical, thermal and electrical properties. Over the past years, multicomponent [2, 3], multi-layered [4, 5], nanostructured [6, 7], superlattice [8, 9], gradient composite architectures [10] have been explored which are beneficially affecting properties of the composite coatings. Thus, it is promising to develop a novel architecture of the composite coating in order to follow the developing trends of the smart coatings.

One-dimensional (1D) fibres reinforced composite architecture is widely used in bulk composite materials, such as the carbon nanotubes reinforced metal matrix composites and ceramic matrix composites [11, 12]. However, limited work has been done on the

1D fibres reinforced composite coatings, because it is difficult to control the dispersion of the 1D reinforcements during the deposition process. To overcome this problem, different strategies have been explored to achieve the well-designed nanocomposite coatings, such as premixing approach, one-step approach, and two-step approach, each approach has its advantages and drawbacks [13-18]. As CNT is a common 1D nanofibers, most of the works on the nanofibres reinforced composite coatings were carried out using CNTs as the reinforcements.

Uniform dispersion of fibres in the matrix is the main challenge in the deposition of the 1D composite coatings. Two typical premixing approaches to achieve mixtures are solution mixing process or ball milling process, respectively [19-23]. Electrochemical or thermal spray techniques were usually applied for the deposition of 1D composite coatings. Pei *et al.* [23] deposited the Single-walled CNT/hydroxyapatite composite coatings on titanium by electrochemical deposition, and both mechanical property and in-vitro bioactivity of the composite coating can be improved. Tan *et al.* [24] prepared the Ni-CNTs composite coatings using brush plating in an attempt to improve the wear resistance of Ni coating, but more pores were produced compared to the brush plated pure Ni coating. Bakshi et al. deposited the CNTs reinforced Al-based composite coating using the cold spray technique, by ball milling process to achieve the powder mixture. However, the ball milling process cannot inhibit the agglomeration of the CNTs and may cause damages on the CNTs [25].

Kinoshita *et al.* [15] investigated mechanical properties of a DLC-CNTs composite coatings deposited with PECVD through a two-step approach. The toughness of the composite coatings was improved. However, DLC did not naturally impregnate the CNTs because of the complex interaction between CNTs and the matrix. Ji et al. developed a two-step deposition approach to acquire the well-designed CNTs reinforced DLC composite coating, and the reinforced CNTs can affect the electrical properties of the composite coating [26]. The key challenge in the two-step approach is to control the fibre template in order to achieve a well dispensed composited structure.

However, it is difficult to achieve the 1D fibres reinforced composite coating through a one-step approach, because the conventional techniques are not feasible to synthesise fibres and matrix simultaneously. Thus, it is expected to develop a novel technique which can obtain the fibres and coating at the same time. Solution based processes have been developed to synthesise metal nanowires, such as Ag nanowires[27, 28], Pt nanowires[29], etc. Those metal nanowires can provide unique properties, such as antibacterial activities (Ag), and catalytic performance (Pt). However, the vapor phase-based methods are not as versatile as the chemical solution-based methods for the synthesis of nanowires, but they provide possibilities for creating the wires reinforced composite coatings, by depositing the fibres and the matrix simultaneously.

The aim of this study is to develop a feasible technique to achieve fibres reinforced 1D composite coating through a one-step approach – active screen plasma (ASP) co-alloying process. The ASP co-alloying technique was applied to deposit the Ag wires

reinforced composite coatings, and the microstructures of the composite coatings were characterised to explain the formation mechanism. Antibacterial performance of this Ag wires reinforced composite coating was tested to explore the potential application of this novel composite coating.

2. Experimental methods

2.1 Materials and deposition methods

The Ag wires reinforced composite coatings were deposited using a DC Klöckner Ionon 40 kVA (Germany) plasma furnace with additional ASP settings placed on the worktable. Samples were put within the active screen and kept at a floating potential by using ceramic insulators above worktable. The ASP settings are similar to that described in our previous work [30]. The schematic diagram of the deposition system is shown in Fig.1. Distance between the silver plate and the stainless-steel (SS) lid is 6 mm, whilst distance between the SS lid and the sample surface varied. The composition of the 316 stainless steel active screen lid is shown in Table 1. This system takes advantages of the allocated heating source from the hollow cathode effect between the Ag lid and the SS lid in order to sputter the Ag particles during the deposition process.

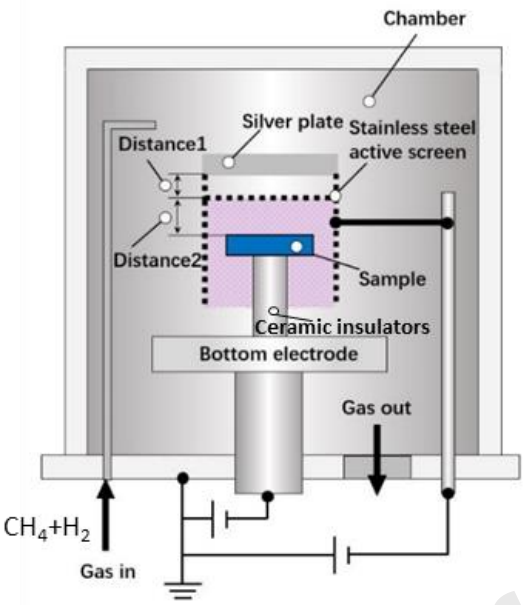

Fig.1 Schematic diagram of the settings for the deposition of the Ag wires reinforced composite coatings. Samples are placed on ceramic insulators and kept at a floating potential. Targets are set on top of the samples which are connected to the top electrode.

Table 1 Chemical composition of the 316 stainless steel active screen lid.

Element	Cr	Ni	Mo	Mn	Si	C	P	S	Fe
Content (wt. %)	17.2	11.7	2.2	1.3	0.6	0.06	0.026	0.014	Balanced

The coating was deposited on the ground AISI 316 SS substrate with the size of Φ25.4×5 mm, the samples to be treated were wet ground with 1200# grit SiC paper to the average roughness of 108±15nm, measured by profilometer and ultrasonically cleaned in acetone. To investigate the influences of the deposition conditions on the formation of Ag wires reinforced composite coatings, a series of experiments were designed and carried out, and the corresponding parameters are listed in Table 2. All of the deposition processes were carried out at 420℃and the total deposition time was 20h. For A3 to A6, the depositions started at the pressure of 1 mbar for 2h and then increase

to 3 mbar for the other 18 h. The plasma was generated from the gas mixture of CH_4 and H_2.

Table 2 Deposition parameters of the active screen plasma co-alloying processes.

Code	Pressure	Temperature	Time	CH_4	H_2	Distance
A1	1 mbar	420℃	20 h	1.5%	98.5%	20mm
A2	3 mbar	420℃	20 h	1.5%	98.5%	20mm
A3	1mbar/3mbar	420℃	2h +18 h	1.5%	98.5%	20mm
A4	1mbar/3mbar	420℃	2h +18 h	3%	97%	20mm
A5	1mbar/3mbar	420℃	2h +18 h	1.5%	98.5%	10mm
A6	1mbar/3mbar	420℃	2h +18 h	1.5%	98.5%	30mm

2.2 Characterisation

Scanning electron microscope (SEM, JEOL 7000) was used to observe the surface and cross-sectional morphologies of the composite coatings and the structures of the Ag wires, equipped with Energy dispersive spectroscopy (EDS) to detect the element distribution with the applied accelerating voltage of 20 kV. X-ray diffraction (XRD) patterns were obtained using an EQUINOX 3000 X-ray Diffractometer (Inel, France) using a Cu Kα radiation source (λ= 1.5406 Å) with the settings of 35kV and 25mA. X-ray photoemission spectroscopy (XPS, ESCALAB 250Xi) was used to investigate the chemical status of the composite surface. Transmission electron microscope (TEM, Oxford JEOL 2100 LaB_6) was utilized to analyse nanostructure and composition of the composite coating at an acceleration voltage of 200 kV. The TEM sample of coating cross-section was prepared *in-situ* with the focused ion beam (FIB) microscopy. The roughness of the composite coatings was measured by Ambios XP-200 stylus profilometer, stylus with a diamond tip scan against the surface to get a 2mm profile

under the load of 1mg with a speed of 0.05mm/s. Each sample was scanned 3 times to obtain the average roughness.

2.3 Antibacterial test

Antibacterial tests were carried out following the JIS Z 2801:2000 bacterial enumeration standard [31]. All samples were sterilized by autoclaving before the antibacterial tests, and commercial glass slides were used as control samples. The test bacteria were cultured in Tryptone soya agar. Basic procedures of the antibacterial tests are schematically shown in Fig. 2. The first step was to dilute the bacteria in broth to decrease the optical density to 0.05 (about 107 cells/ml), and then the diluted suspensions were pipetted on the surfaces of the samples, which were covered by sterile glass coverslips to ensure the equal contact areas on each sample. Samples were then put inside the Petri dishes and incubated for 5h at room temperature. Step two is to collect the bacteria. The samples were washed by 10 ml of sterile phosphate buffered saline (PBS) within a sterile container. The dislodge process was carried out with a vortex mixer for 10s. During the following step three, the diluted bacteria suspension (100 μl) was pipetted on the Tryptone soya agar plate and incubated at 37°C for 24 h. The last step is to count the number of the colony forming units (CFU δ_{CFU}) on the Petri dish,equal to the value of the surviving bacterial cells after step one, and used to calculate the killing rate.

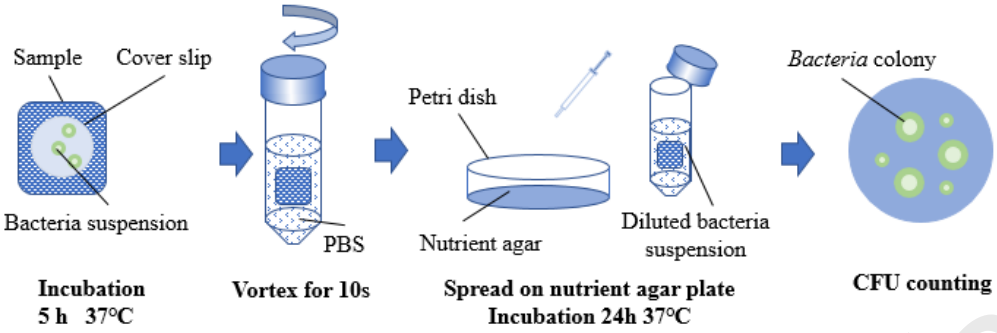

Fig. 2 Schematic diagram of the antibacterial test procedures.

3. Results

3.1 Surface morphologies

The morphologies of the composite coatings deposited by the ASP technique are shown in Fig. 3, which are significantly influenced by the deposition conditions. Fig. 3(a) shows the surface morphology of the composite coating synthesised at 1 mbar for 20h (A1). It can be seen that some particles are distributed on the surface of the substrate, which may due to the strong hollow cathode effect under the low gas pressure, and hence lots of stainless-steel nanoparticles and Ag particles were sputtered off from the active screen lids, but no continuous coating was formed in this case.

For the coating deposited at 3 mbar for 20 h (A2), large agglomerations can be clearly seen on the sample surface. These particles are much bigger than that formed under A1 condition. Large Ag aggregates could be observed on the surface of the A2 composite coating. When the pressure is changed, a wire-shaped structure embedded in the matrix of the composite coating can be observed from the surface of A3 composite coating in Fig. 3(c). The length of these wires varies from 1 to 10 μm. However, it is difficult to measure the diameter and length of the Ag wires accurately, because some of the Ag

wires were embedded in the matrix. These wires are mainly formed with Ag as verified by EDS. Fig. 3(d) presents the surface morphology of the A4 composite coating synthesized with an increased fraction (3%) of methane. Ag wires were also formed during the deposition process, but a thick carbon-rich layer seems to be formed due to the high amount of carbon source. Although the growth mechanism of the Ag wires during the sputtering process is not fully understood, these SEM observations indicate that the deposition conditions for A3 and A4 provided suitable conditions for the growth of Ag wires, and a lower percentage of methane (1.5%) would produce a uniform Ag wires reinforced composite coating.

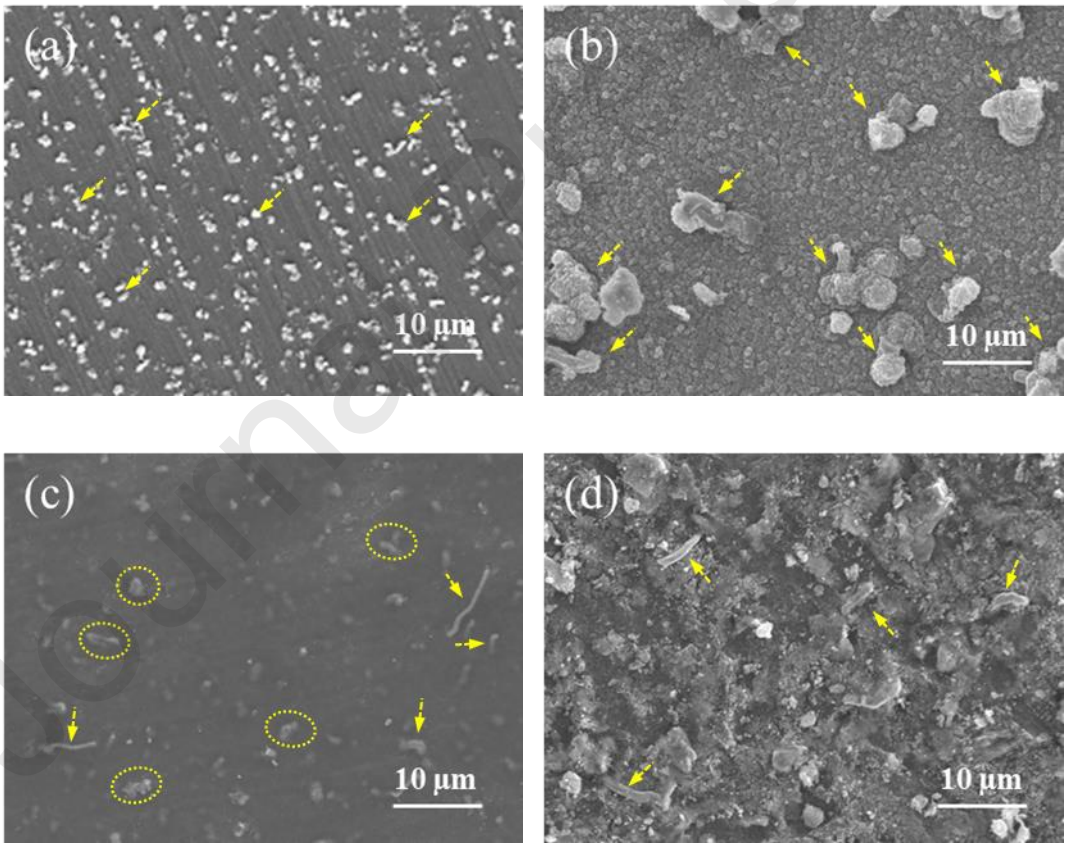

Fig. 3 Surface morphologies of the composite coating deposited by ASP technique under different parameters: (a) low pressure 1 mbar A1; (b) high pressure 3 mbar A2; (c) 1 mbar/3 mbar and 1.5% methane A3; (d) 1 mbar/3 mbar and 3% methane A4. The yellow arrow marks point to the Ag wires or aggregates on the surfaces, and the yellow circles mark the Ag wires or aggregates within the matrix.

These explorations above have revealed that the Ag wires reinforced composite coating deposited under A3 conditions exhibited a good Ag wire reinforced composite structure. Thus, composite coatings A5 and A6 are deposited using similar deposition parameters but under different deposition distances. The surface morphologies and cross-section view of A3, A5 and A6 composite coatings are compared in Fig. 4. It shows that the deposition distance has limited influence on the formation of the Ag wires. However, the diameter and length of the Ag wires are not uniform, some parts of the Ag wires were curled in the composite coating, diameters of the Ag wires ranged from 400nm to 1300nm. The diameter variation of these curly Ag wires implies that these Ag wires are likely not a single crystal, which is different from those single crystalline Ag nanowires grown through the chemical process [28, 32].

Fig. 4 (b)&(d)&(e) show the cross-section views of the composite coatings, and their thicknesses are around 2.11 μm (A3), 3.04 μm (A5) and 1.87 μm (A6), respectively. This indicates that a shorter deposition distance would lead to a thicker composite coating. Besides, the A3 & A5 composite coatings exhibit good adhesion to the substrate after the grinding process, while the A6 composite coating is partially delaminated just after the sample preparation, indicating that a long deposition distance can reduce the adhesion of the composite coating to the substrate.

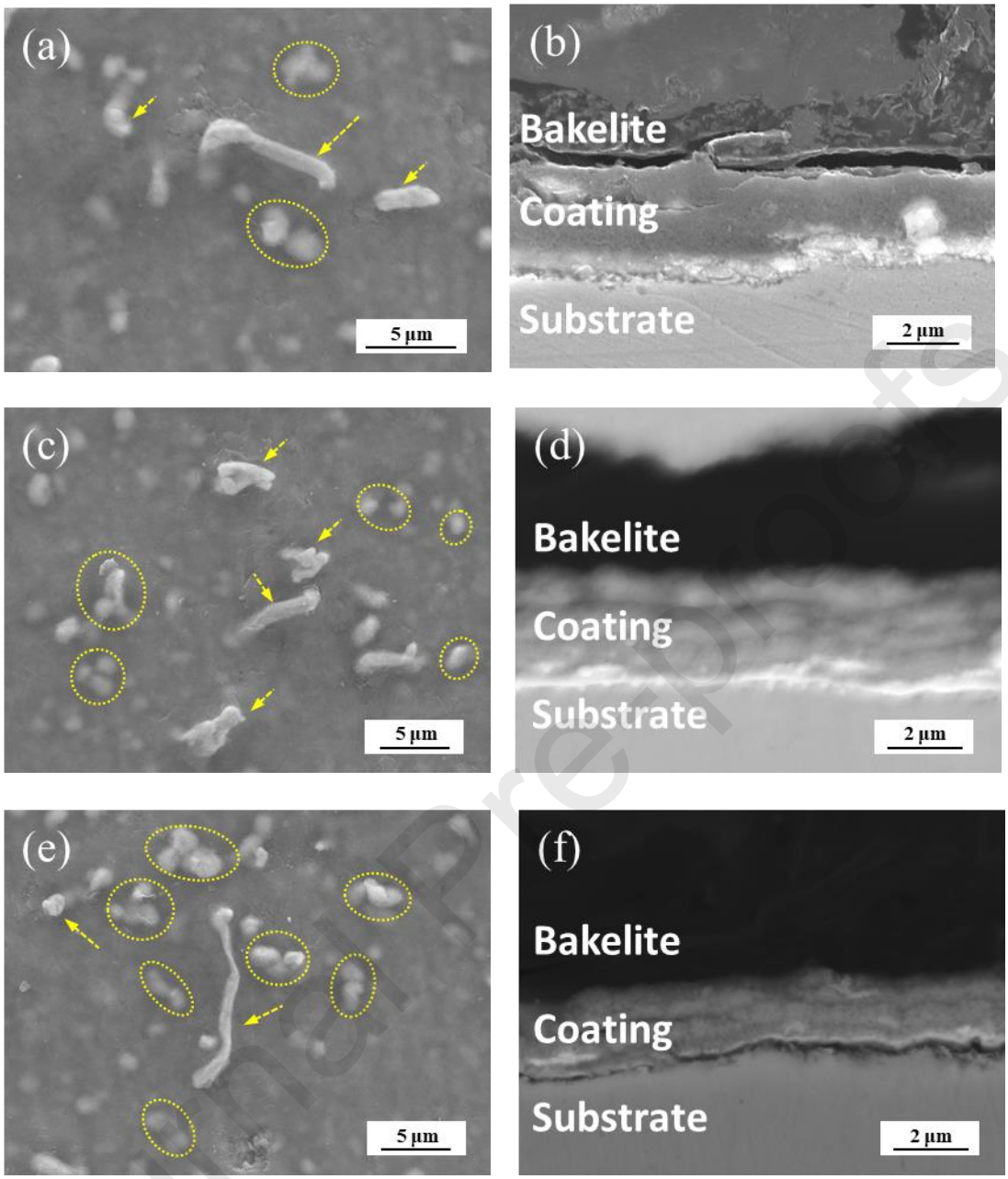

Fig. 4 Surface morphologies and cross-section views of the Ag wires reinforced composite coatings. A3: (a) & (b); A5: (c) & (d); A6: (e) & (f). The yellow arrow marks point to the Ag wires on the surfaces, and the yellow circles mark the Ag wires or aggregates within the matrix.

3.2 XRD analysis

The phase components of the composite coatings (A3, A5, A6) and the SS substrate were investigated by XRD and the corresponding spectra are shown in Fig. 5. Typical

peaks (111), (200) and (220) of the γ-phase for the face-centred cubic (fcc) structured austenitic stainless steel were detected from the 316 SS substrate. As shown in Fig. 5, the XRD patterns of the composite coatings (A3, A5, A6) present similar peaks, indicating that the change of the deposition distance does not affect the phases of composite coatings. The γ-phase peaks were also detected from the Ag reinforced composite coating, which may generate from the composite coating and the substrate. No peaks for chromium carbides were detected, which indicates that the sputtered SS nanoparticles did not react with the carbon precursor during the deposition process at 420℃. Beside the γ-phase, peaks at around 38.2°, 44.5°, 64.7°, 77.7° and 82.0° can match the (111), (200), (220), (222), and (311) peaks for pure fcc Ag, indicating both the Ag wires and the Ag nanoparticles in the composite coating are still in pristine status.

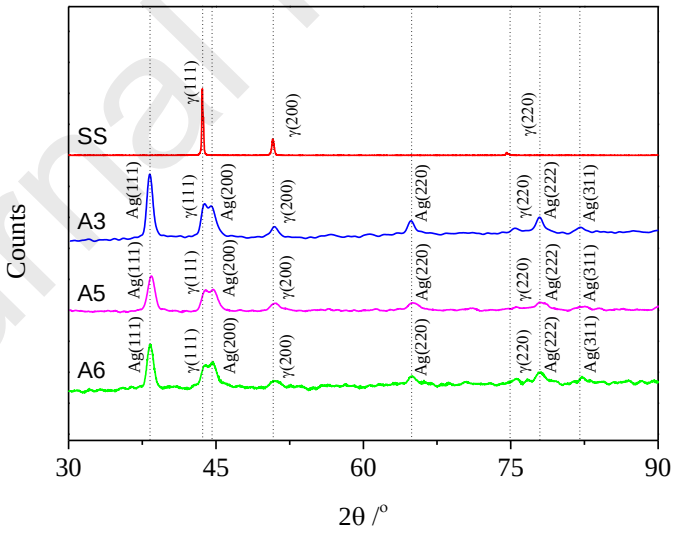

Fig. 5 XRD results of the untreated 316 stainless steel and the A3 composite coating with Ag wires.

3.3 XPS analysis

The surface chemical states of the Ag wire reinforced A3 composite coating have been investigated by X-ray photoelectron spectroscopy (XPS). The spectra were collected from the as-deposited surface and the sublayer after etching for 60s by Ar ions, in order to compare the chemical state variation of the composite coating. Fig. 6 shows the survey spectra and high-resolution spectra of Ag 3d, C 1s and Fe 2p. The survey spectra are shown in Fig. 6(a) indicates that the chemical states are different before and after etching. After etching, more peaks were detected from the surface which indicates that there is an oxide layer formed at the surface and an obvious peak for O 1s can be viewed from the unetched surface (see Fig. 6(a)).

Fig. 6(b) shows the high-resolution Ag spectra from the composite coating. Peaks belong to Ag $3d_{5/2}$ at 368.2 eV and Ag $3d_{3/2}$ at 374.3 eV were detected from the coating surface before and after etching. These two peaks prove that the Ag detected from the composite coating has a valence of zero, indicating that the wires are formed with pure Ag.

Fig. 6(c) shows the C 1s spectra of the composite coating. The peak at 284.6 eV detected from both the unetched and the etched coating surface can be assigned to the C-C bond. Besides, a shoulder peak at 286.2 eV corresponding to the C-O bond was only detected from the unetched surface, which may be due to the reactions between the surface carbon and oxygen in the ambient, while no such C-O peak can be detected from the composite coating after etching.

Fig. 6(d) shows the high-resolution spectra of iron, and very weak peaks for Fe were detected before etching. Clear peaks at 706.7 eV and 720.0 eV are corresponding to Fe^0, indicating that the SS nanoparticles had not reacted with the carbon during the deposition process, which is consistent with the XRD results.

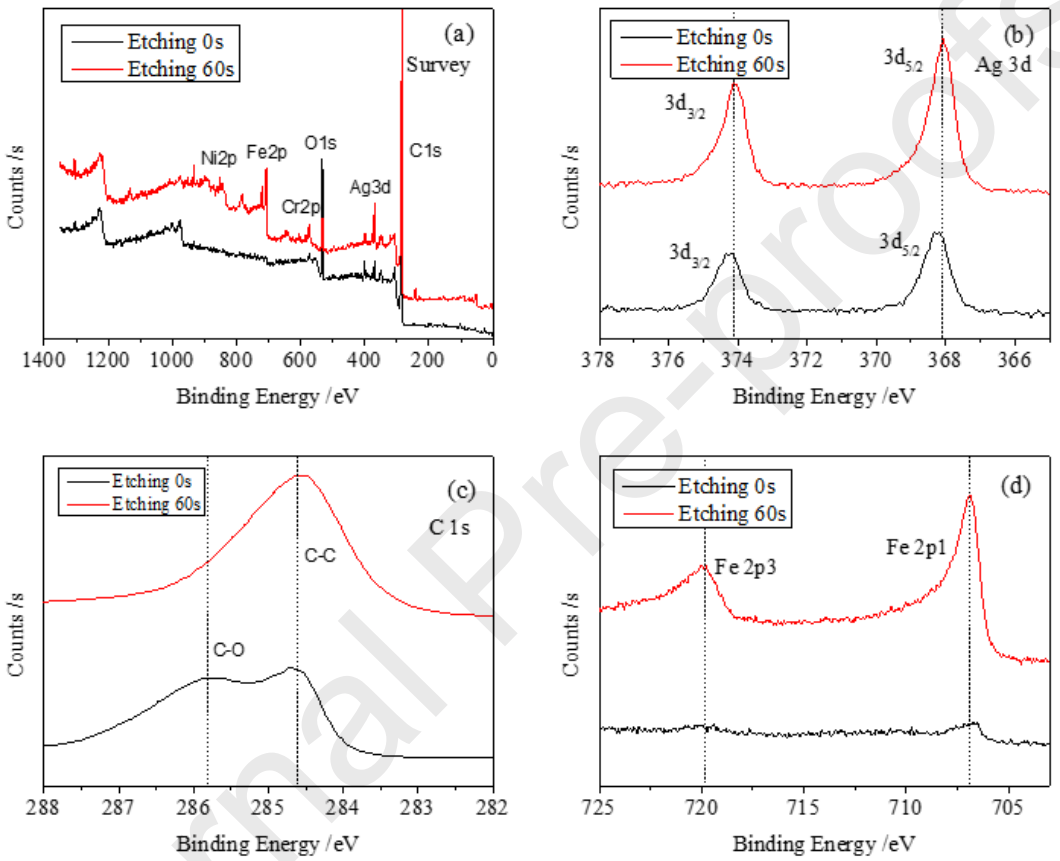

Fig. 6 XPS spectra of the Ag wire reinforced composite coating (A3). (a) survey of the Ag wire reinforced composite coating; (b) Ag 3d spectra; (c) C 1s spectra; (d) Fe 2p spectra

3.4 Raman spectroscopy

In order to investigate the microstructures of these carbon-rich composite coatings, Raman analysis has been conducted and the Raman spectra are shown in Fig. 7. D peak and G peak at around 1355 cm^{-1} and 1590 cm^{-1} respectively were detected from all those composite coatings. The high intensity of D peak indicates that there are lots of

defects formed in the coatings during the plasma deposition process. Unlike a typical diamond-like carbon films which usually have overlapped D peak and G peak [33], the D peak and G peak, in this case, are separated from each other, indicating that carbon in these composite coatings has a different structure as compared with the hard amorphous carbon.

No peak shift was observed from these Raman spectra on different samples due to the similar deposition processes. However, the band intensity ratios (I_D/I_G) of the composite coatings are varied from 1.02 to 1.15. It is known that the band intensity ratios (I_D/I_G) are an indication of defects in the coatings. The experimental results have revealed that a high-intensity ratio can be generated when the deposition processes were carried out with a high percentage of methane (A4) or with a small deposition distance (A5).

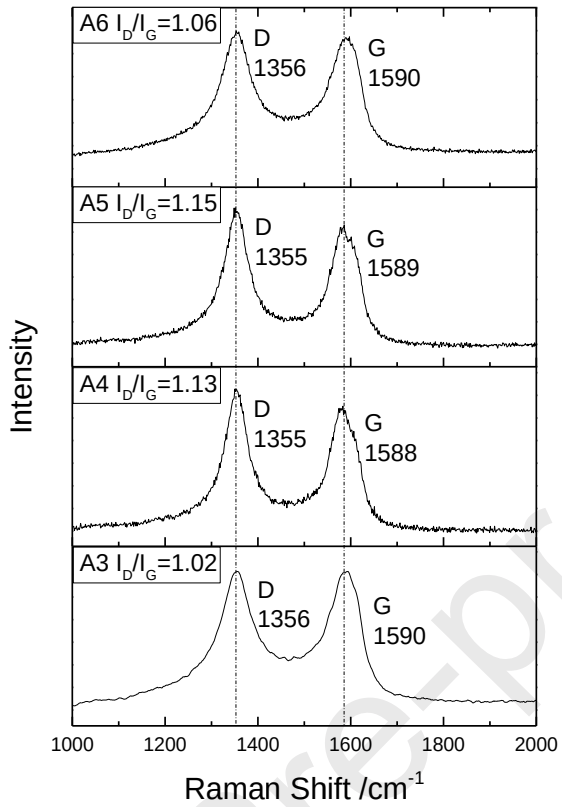

Fig. 7 Raman spectra of the Ag wires reinforced composite coatings (A3, A4, A5 and A6). The positions of D peak and G peak are marked, and the intensity ratios are calculated and presented in the image

3.5 TEM analysis

TEM was utilised to investigate the microstructure of the composite coating. The cross section TEM sample of the composite coating was prepared by FIB as shown in Fig. 8(a). However, it is difficult to capture the cross-section samples of the Ag wire, which due to its shape can easily fall out of the matrix during the etching process. The as-deposited TEM sample mainly shows the microstructures of the matrix. Fig. 8(b) shows the bright field image of the matrix and the EDS results confirmed that the matrix was formed with Ag, SS and carbon. It can be seen that the matrix is formed with

crystallites in nanoscale, ranging from 10 nm to 100 nm. The selected area electron diffraction (SAED) pattern of this area is inserted in Fig. 8(b), several ring diffraction patterns can be observed and some discrete spots in the ring patterns indicate that these nanoparticles are single crystalline and they are oriented along with specific directions [34]. The analysis of the SAED pattern indicates that the ring diffraction patterns are mainly generated by Ag nanograins and austenitic stainless-steel nanograins. However, the interplanar spacings of these two materials belong to the same family (h,k,l) which are close to each other. Thus, there are two series of face-centered cubic (fcc) crystals ring diffraction patterns can be identified which belong to Ag nanograins and austenitic stainless-steel nanograins. TEM results indicate that the silver and austenitic stainless-steel nanoparticles are still in their pristine status, which are consistent with the XRD and XPS results.

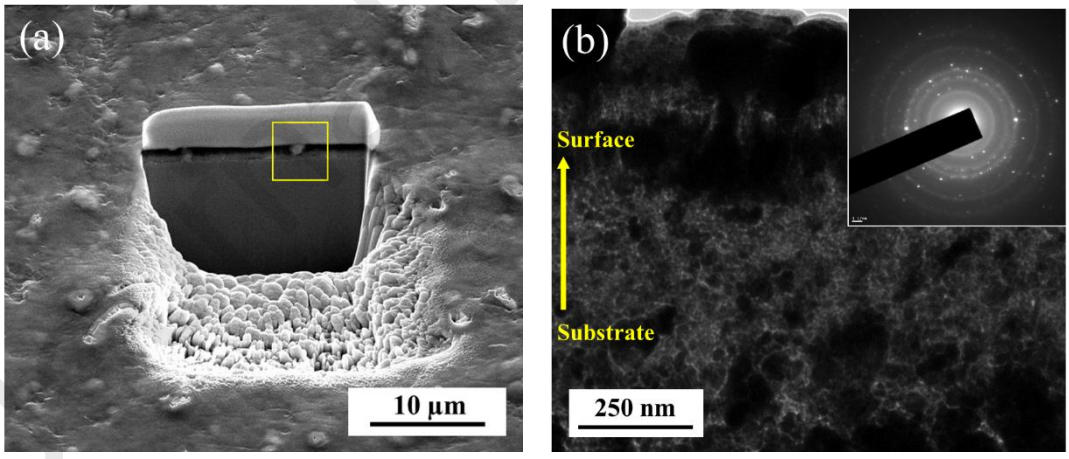

Fig. 8 (a) SEM image of the composite coating etched by FIB for preparation of TEM sample. (b) TEM image of the matrix of the composite coating, and insert image shows the SAED ring pattern of the matrix (A3).

3.6 Wettability and hardness

The contact angle of the Ag wires reinforced composite coatings were measured to evaluate their wettability, which is influenced by the physical and chemical status of the surfaces. As shown in Fig. 9(a), the polished stainless-steel substrate surface presents a 96º contact angle which is relatively hydrophobic, while the contact angles of the Ag wires reinforced composite coatings are 55º, 59º, and 63º for A3, A5, A6, respectively. This indicates that these composite surfaces are hydrophilic. The variations of contact angles between the composite surfaces may be caused by the roughness, and the corresponding average roughness (Ra) of the composite coatings are 573±55 nm (A3), 616±58 nm (A5) and 551±50 nm (A6), respectively, as compared to the ground stainless-steel substrate roughness of 85 ±12 nm.

The microhardness of the Ag wires reinforced composite coatings are measured under the load of 50g. Fig. 9(b) shows that the hardness of the composite surfaces (~500 $HV_{0.05}$) is higher than that of the stainless-steel substrate (~245 $HV_{0.05}$). The hardness enhancement of the composite surface may be due to the diffusion of carbon into the substrate.

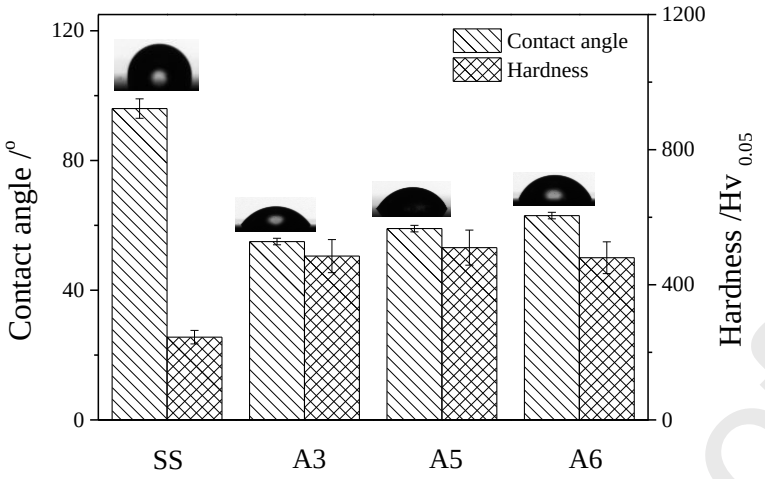

Fig. 9 Contact angles between distil water and the different surfaces to evaluate the wettability of the composite surfaces, and optical images of the water droplets are inserted

3.7 Antibacterial properties

Antibacterial tests were carried out to evaluate the bacterial inhibition performance of the Ag wires impregnated composite coatings. Both Gram-negative *P. gingivalis* and Gram-positive *S. epidermidis* bacteria were used to study the antibacterial effect of the Ag wires impregnated composite surfaces.

Fig. 10(a)&(b) shows the colonies of the Gram-negative *P. gingivalis* on the tryptone soya agar plates after incubation. Each spot inside the plate stands for one colony of *P. gingivalis*. As there is no antibacterial effect of the glass slide control sample, most of the *P. gingivalis* are alive after 5h contact. As such, a lawn of *P. gingivalis* colonies formed, which almost cover the whole agar plate, as revealedin Fig. 10(a). In contrast, Fig. 10(b) shows the colonies of *P. gingivalis* after contact with the Ag impregnated composite coating. The number of colonies is much less compared to that of the control, indicating the inhibition effect of the composite coating. The colonies in each plate were

counted to calculate the antibacterial efficiency of the Ag impregnated composite coating to *P. gingivalis* and the quantitative results are shown in Fig. 10(e) (92.2%).

In addition to the Gram-negative bacteria (*P. gingivalis*), Gram-positive bacteria (*S. epidermidis*) was also used to study the antibacterial activity of the Ag wires reinforced composite coating. Fig. 10(c)&(d) shows the *S. epidermidis* colonies on the soya agar plates after the antibacterial tests. The test conditions are as same as the antibacterial tests to *P. gingivalis*. The colonies of *S. epidermidis* after contact with the control glass are not killed therefore spread over the whole soya agar plate as shown in Fig. 10(c), the size of the *S. epidermidis* colonies is lager compared to that of the *P. gingivalis* colonies. On the other hand, a few colonies of *S. epidermidis* are shown in Fig. 10(d), because they were incubated from the suspension after contact with the Ag impregnated coating. The antibacterial efficiency of the composite coating to *S. epidermidis* is 95%, which is slightly higher compared to that of the P. gingivalis (Fig. 10(e)).

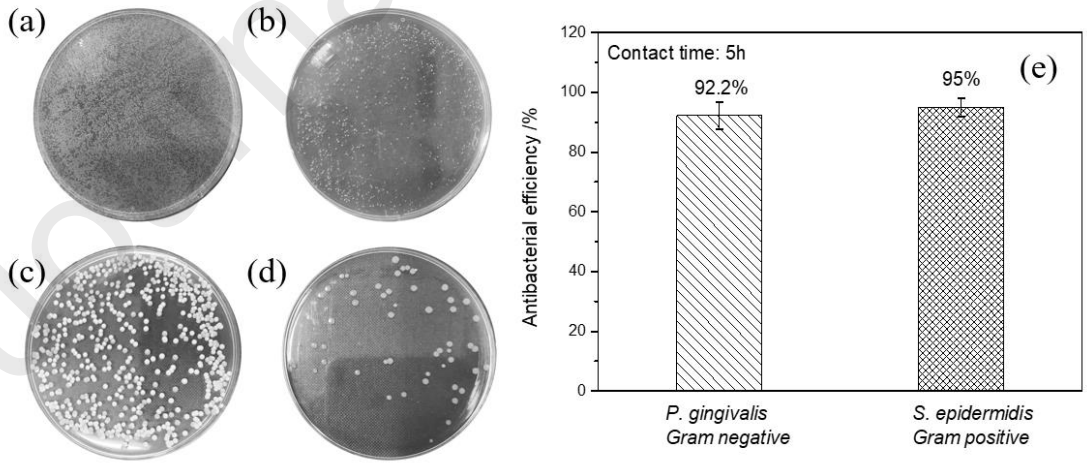

Fig. 10 *P. gingivalis* colonies on the soya agar plates after 5 h contact with (a) glass and (b) Ag impregnated composite coating; S. epidermidis colonies on the soya agar plates after 5 h contact with (c) glass and (d) Ag impregnated composite coating; (e) Antibacterial efficiency of the Ag impregnated composite coating against both Gram-negative P. gingivalis and Gram-positive S. epidermidis.

3.8 Formation mechanism of the Ag wires

The Ag wires reinforced composite coating was deposited by the low-temperature ASP process in an ambient of methane and hydrogen. However, the growth mechanism of the silver wires is still not fully understood. Different strategies have been developed to synthesise the 1D metal wires, such as spontaneous growth [35], template-based growth [36], and lithography [37]. The spontaneous growth of wires is commonly driven by the reduction of Gibbs free energy or chemical potential, and it can be typically categorized into (a) vapor phase growth and (b) solution-based growth. Anisotropic growth is required for the formation of the 1D structure which means that the crystal grows faster along one direction than others.

The oxide-assisted, vapor-liquid-solid (VLS) and vapor-solid (VS) were applied to explain the growth of metal nanowires through vapor phase growth [38-42]. In the present study, as there was no oxygen in the reaction ambient, the oxide-assisted growth mechanism cannot be used to explain the formation of Ag wires [38, 39]. The VLS mechanism can also be excluded because the typical characteristic of the VLS mechanism is the presence of catalyst particles or globules at the end of the wires due to the supersaturation, and the process is usually carried under high temperature [40, 41]. However, no catalysts were used in our synthesis process and the SEM images showed that no droplets capped at the end of the Ag wires. Therefore, according to the processing and characterisation analysis, the formation of the solid Ag wires can be explained by a vapor-solid (VS) growth mechanism which involves nucleation and growth processes [42, 43]. A schematic diagram of the growth mechanism of Ag wires

is presented in Fig. 11. The Ag nanoclusters were generated during the sputtering process, and these Ag ion nanoclusters are the building units which serve as seeds for the subsequent growth. The aggregates formed by the Ag ion nanoclusters underwent collision and coalescence in the plasma field. The further growth of the aggregates will align themselves into a crystal structure to decrease the interfacial energy, and eventually to form a nanowire structure. The anions will be continuously absorbed onto the surface of the nanowire which induces the axial growth and radial growth. The axial growth would be ceased due to a depletion of Ag in the adsorption layer [44]. Besides, the continuous sputtering of Ag and SS nanoparticles and the condensation of carbon would result in the formation of the Ag wires reinforced composite coating.

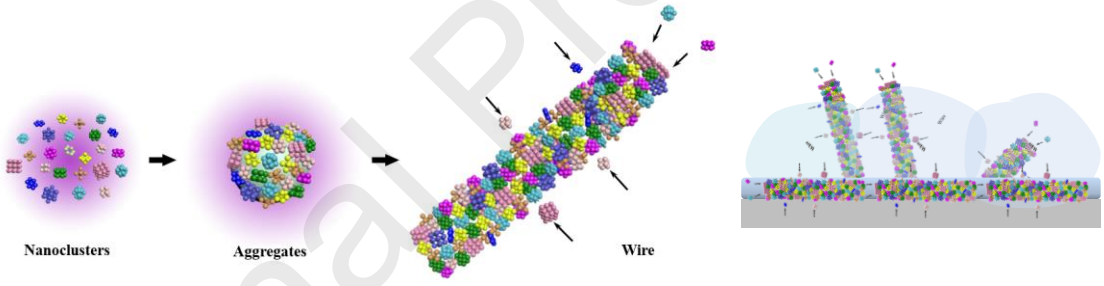

Fig. 11 Schematic diagram of the growth mechanism of the Ag wires, the sputtered Ag nanoclusters were aggregated first and then grew anisotropically to form the Ag wire.

4. Conclusions

A novel ASP approach has been developed for the *in-situ* synthesis of Ag wires and wires reinforced composite coating in a plasma ambient of methane and hydrogen. The average diameter and length of as deposited Ag wires are around 500 nm and 5 μm, which are randomly embedded in the composite coating. The matrix is mainly formed

with Ag nanoparticles, SS nanoparticles and carbon, whilst no compounds were formed between the sputtered nanoparticles and carbon which was proved by XRD, XPS, and TEM. This composite surface is relative hydrophilic with a water contact angle around 60^{o}, and its hardness is elevated due to the diffusion of carbon. Excellent antibacterial performances against both Gram-negative *P. gingivalis* (92.2%) and Gram-positive *S. epidermidis* (95%) were achieved by this Ag contained composite coating after 5h contact.

Acknowledgements

The authors wish to express their appreciation to the financial support of the EC H2020-MODCOMP project (Grant No. GA685844) and National Key R&D Program of China (2017YFB0310703, 2017YFF0207905)

Reference

[1] C. Donnet, A. Erdemir, Historical developments and new trends in tribological and solid lubricant coatings, Surf. Coat. Technol., 180 (2004) 76-84.

[2] L. Wang, Y.B. He, L. Shen, D. Lei, J. Ma, H. Ye, K. Shi, B. Li, F. Kang, Ultra-small self-discharge and stable lithium-sulfur batteries achieved by synergetic effects of multicomponent sandwich-type composite interlayer, Nano Energy, 50 (2018) 367-375.

[3] A. Laszczyńska, J. Winiarski, B. Szczygieł, I. Szczygieł, Electrodeposition and characterization of Ni–Mo–ZrO2 composite coatings, Appl. Surf. Sci., 369 (2016) 224-231.

[4] B.S. Xu, Y. Du, P. Wang, L.W. Yan, B.Q. Sun, B. Du, Y.H. Cheng, C.Q. Hong, Microstructure, surface emissivity and ablation resistance of multilayer coating for lightweight and porous carbon-bonded carbon fiber composites, J. Alloys Compd., 685 (2016) 799-805.

[5] J. Xiang, L. Ma, H. Su, J. Xiong, K. Li, Q. Xia, G. Liu, Layer-by-layer assembly of antibacterial composite coating for leather with cross-link enhanced durability against laundry and abrasion, Appl. Surf. Sci., 458 (2018) 978-987.

[6] S. Kim, U.T. Jung, S.K. Kim, J.H. Lee, H.S. Choi, C.S. Kim, M.Y. Jeong, Nanostructured Multifunctional Surface with Antireflective and Antimicrobial Characteristics, ACS Appl. Mater. Interfaces, 7 (2015) 326-331.

[7] W. Wu, W. Chen, S. Yang, Y. Lin, S. Zhang, T.-Y. Cho, G.H. Lee, S.-C. Kwon, Design of AlCrSiN multilayers and nanocomposite coating for HSS cutting tools, Appl. Surf. Sci., 351 (2015) 803-810.

[8] A. Oila, S.J. Bull, Experimental assessment of the elastic properties of thin TiN/AlN superlattice and nano-multilayer coatings, Surf. Coat. Technol., 257 (2014) 87-94.

[9] J. Pu, D. He, L. Wang, Effects of WC phase contents on the microstructure, mechanical properties and tribological behaviors of WC/a-C superlattice coatings, Appl. Surf. Sci., 357 (2015) 2039-2047.

[10] H. Lin, W. Liang, Y. Jia, Q. Miao, R. Hu, Z. Ding, L. Yu, Effect of AlY gradient coating on hot corrosion resistance of γ-TiAl alloy at different temperatures, Appl. Surf. Sci., 487 (2019) 868-875.

[11] S.R. Bakshi, D. Lahiri, A. Agarwal, Carbon nanotube reinforced metal matrix composites - a review, Int. Mater. Rev., 55 (2010) 41-64.

[12] S.H. Dong, J.Q. Zhou, D. Hui, Y. Wang, S. Zhang, Size dependent strengthening mechanisms in carbon nanotube reinforced metal matrix composites, Composites Part a-Applied Science and Manufacturing, 68 (2015) 356-364.

[13] F. Li, Y. Liu, C.B. Qu, H.M. Xiao, Y. Hua, G.X. Sui, S.Y. Fu, Enhanced mechanical properties of short carbon fiber reinforced polyethersulfone composites by graphene oxide coating, Polymer, 59 (2015) 155-165.

[14] G. Archambault, B. Jodoin, S. Gaydos, M. Yandouzi, Metallization of carbon fiber reinforced polymer composite by cold spray and lay-up molding processes, Surf. Coat. Technol., 300 (2016) 78-86.

[15] H. Kinoshita, I. Ippei, H. Sakai, N. Ohmae, Synthesis and mechanical properties carbon nanotube/diamond-like carbon composite films, Diam Relat Mater, 16 (2007) 1940-1944.

[16] D. Varshney, A.V. Sumant, B.R. Weiner, G. Morell, Growth of carbon nanotubes on spontaneously detached free standing diamond films and their field emission properties, Diam. Relat. Mater., 30 (2012) 42-47.

[17] H.Y. Hu, G. Chen, J.Y. Zha, Facile synthesis of CNTs-doped diamond-like carbon film by electrodeposition, Surf. Coat. Technol., 202 (2008) 5943-5946.

[18] K. Guan, L. Zhang, F. Zhu, H. Sheng, H. Li, Surface modification for carbon/carbon composites with Mg-CaP coating reinforced by SiC nanowire‐carbon nanotube hybrid for biological application, Appl. Surf. Sci., 489 (2019) 856-866.

[19] S. Arai, T. Osaki, M. Hirota, M. Uejima, Fabrication of copper/single-walled carbon nanotube composite film with homogeneously dispersed nanotubes by electroless deposition, Materials Today Communications, 7 (2016) 101-107.

[20] D. Kaewsai, A. Watcharapasorn, P. Singjai, S. Wirojanupatump, P. Niranatlumpong, S. Jiansirisomboon, Thermal sprayed stainless steel/carbon nanotube composite coatings, Surf. Coat. Technol., 205 (2010) 2104-2112.

[21] D.G. Liu, J. Sun, Z.X. Gui, K.J. Song, L.M. Luo, Y.C. Wu, Super-low friction nickel based carbon nanotube composite coating electro-deposited from eutectic solvents, Diam. Relat. Mater., 74 (2017) 229-232.

[22] A.K. Shukla, N. Nayan, S.V.S.N. Murty, K. Mondal, S.C. Sharma, K.M. George, S.R. Bakshi, Processing copper-carbon nanotube composite powders by high energy milling, Mater. Charact., 84 (2013) 58-66.

[23] X. Pei, Y. Zeng, R. He, Z. Li, L. Tian, J. Wang, Q. Wan, X. Li, H. Bao, Single-walled carbon nanotubes/hydroxyapatite coatings on titanium obtained by electrochemical deposition, Appl. Surf. Sci., 295 (2014) 71-80.

[24] J. Tan, T. Yu, B. Xu, Q. Yao, Microstructure and wear resistance of nickel-carbon nanotube composite coating from brush plating technique, Tribol Lett, 21 (2006) 107-111.

[25] S.R. Bakshi, V. Singh, S. Seal, A. Agarwal, Aluminum composite reinforced with multiwalled carbon nanotubes from plasma spraying of spray dried powders, Surf. Coat. Technol., 203 (2009) 1544-1554.

[26] X. Ji, X. Li, H. Yu, W. Zhang, H. Dong, Study on the carbon nanotubes reinforced nanocomposite coatings, Diam. Relat. Mater., 91 (2019) 247-254.

[27] P.Y. Silvert, R. HerreraUrbina, N. Duvauchelle, V. Vijayakrishnan, K.T. Elhsissen, Preparation of colloidal silver dispersions by the polyol process .1. Synthesis and characterization, J. Mater. Chem., 6 (1996) 573-577.

[28] Y.G. Sun, B. Gates, B. Mayers, Y.N. Xia, Crystalline silver nanowires by soft solution processing, Nano Lett., 2 (2002) 165-168.

[29] S. Du, A Facile Route for Polymer Electrolyte Membrane Fuel Cell Electrodes with in situ Grown Pt Nanowires, J. Power Sources, 195 (2010) 289-292.

[30] X.C. Ji, W. Zhang, X.Y. Li, H.L. Yu, H.S. Dong, A novel hybrid method combining ASP with PECVD for in-situ low temperature synthesis of vertically aligned carbon nanotube films, Diam. Relat. Mater., 77 (2017) 16-24.

[31] S. Suzuki, S. Imai, H. Kourai, Background and evidence leading to the establishment of the JIS standard for antimicrobial products, Biocontrol Sci., 11 (2006) 135-145.

[32] Y.G. Sun, Y.D. Yin, B.T. Mayers, T. Herricks, Y.N. Xia, Uniform silver nanowires synthesis by reducing AgNO3 with ethylene glycol in the presence of seeds and poly(vinyl pyrrolidone), Chem. Mater., 14 (2002) 4736-4745.

[33] A. Modabberasl, P. Kameli, M. Ranjbar, H. Salamati, R. Ashiri, Fabrication of DLC thin films with improved diamond-like carbon character by the application of external magnetic field, Carbon, 94 (2015) 485-493.

[34] P. Kouvaris, A. Delimitis, V. Zaspalis, D. Papadopoulos, S.A. Tsipas, N. Michailidis, Green synthesis and characterization of silver nanoparticles produced using Arbutus Unedo leaf extract, Mater. Lett., 76 (2012) 18-20.

[35] U. Cvelbar, Z.Q. Chen, M.K. Sunkara, M. Mozetic, Spontaneous Growth of Superstructure alpha-Fe2O3 Nanowire and Nanobelt Arrays in Reactive Oxygen Plasma, Small, 4 (2008) 1610-1614.

[36] W.C. Lee, K. Kim, J. Park, J. Koo, H.Y. Jeong, H. Lee, D.A. Weitz, A. Zettl, S. Takeuchi, Graphene-templated directional growth of an inorganic nanowire, Nat. Nanotechnol., 10 (2015) 423-428.

[37] A. Chauvin, N. Stephant, K. Du, J.J. Ding, I. Wathuthanthri, C.H. Choi, P.Y. Tessier, A.A. El Mel, Large-Scale Fabrication of Porous Gold Nanowires via Laser Interference Lithography and Dealloying of Gold-Silver Nano-Alloys, Micromachines, 8 (2017).

[38] N. Wang, Y.H. Tang, Y.F. Zhang, C.S. Lee, S.T. Lee, Nucleation and growth of Si nanowires from silicon oxide, Physical Review B, 58 (1998) 16024-16026.

[39] W.S. Shi, Y.F. Zheng, N. Wang, C.S. Lee, S.T. Lee, A general synthetic route to III-V compound semiconductor nanowires, Adv. Mater., 13 (2001) 591-+.

[40] Y.Y. Wu, P.D. Yang, Direct observation of vapor-liquid-solid nanowire growth, J. Am. Chem. Soc., 123 (2001) 3165-3166.

[41] R.S. Wagner, W.C. Ellis, Vapor-Liquid-Solid Mechanism of Single Crystal Growth (New Method Growth Catalysis from Impurity Whisker Epitaxial + Large Crystals Si E), Appl. Phys. Lett., 4 (1964) 89-&.

[42] Y.L. Chueh, M.W. Lai, J.Q. Liang, L.J. Chou, Z.L. Wang, Systematic study of the growth of aligned arrays of alpha-Fe2O3 and Fe3O4 nanowires by a vapor-solid process, Adv. Funct. Mater., 16 (2006) 2243-2251.

[43] A. Umar, S.H. Kim, Y.S. Lee, K.S. Nahm, Y.B. Hahn, Catalyst-free large-quantity synthesis of ZnO nanorods by a vapor-solid growth mechanism: Structural and optical properties, J. Cryst. Growth, 282 (2005) 131-136.

[44] Y.D. Yin, G.T. Zhang, Y.N. Xia, Synthesis and characterization of MgO nanowires through a vapor-phase precursor method, Adv. Funct. Mater., 12 (2002) 293-298.

Credit Author Statement

Xiaochao Ji: Conceptualization, Methodology, Validation, Investigation, Writing – original draft, Writing – review and editing

Yangchun Dong: Methodology, Validation, Writing – review and editing

Xiaoying Li: Conceptualization, Methodology

Helong Yu: Funding acquisition

Tian Ma: Conceptualization, Writing – review and editing

Wei Zhang: Supervision

Hanshan Dong: Supervision, Funding acquisition

Declaration of interests

☒ The authors declare that they have no known competing financial interests or personal relationships that could have appeared to influence the work reported in this paper.

☐The authors declare the following financial interests/personal relationships which may be considered as potential competing interests: